Reconnection Driven Lobe Convection: Interball Tail Probe Observations and Global Simulations

Joachim Raeder

Institute of Geophysics and Planetary Physics
University of California, Los Angeles

O. Vaisberg[1], V. Smirnov, and L. Avanov

Space Research Institute
Russian Academy of Sciences, Moscow, Russia
[1] *also at: Space Science Department, NASA Marshall Space Flight Center*
Huntsville, Alabama

Abstract

We present Interball Tail Probe observations from the high latitude mid-tail magnetopause which provide evidence of reconnection between the IMF and lobe field lines during a 6 hour interval of stable northward and dawnward IMF on October 19, 1995. Results from a global magnetohydrodynamic simulation for this interval compare well with the Interball observations. With the simulations we provide an extended global view of this event which gives us insight into the reconnection and convection dynamics of the magnetosphere. We find that reconnection occurs in a region of limited spatial extent near the terminator and where the IMF and the lobe field are anti-parallel. Reconnected IMF field lines drape over the dayside magnetosphere, convect along the flanks into the nightside, and enter the magnetotail in a small entry window that is located in the flank opposite to the reconnection site. Ionospheric convection is consistent with previous observations under similar IMF conditions and exhibits a two cell pattern with a dominant lobe cell over the pole. The magnetic mapping between the ionosphere and the lobe boundary is characterized by two singularities: The narrow entry window in the tail maps to a six hour wide section of the ionospheric lobe cell. A singular mapping line cuts the lobe cell open and maps to almost the entire tail magnetopause. By this singularity the magnetosphere avoids to have a stagnation point, i.e., the lobe cell center, map to a tailward convecting field line. The existence of singularities in the magnetic mapping between the ionosphere and the tail has important implications for the study of tail-ionosphere coupling via empirical magnetic field models. Because the lobe-IMF reconnection cuts away old lobe flux and replaces it with flux tubes of magnetosheath origin solar wind plasma enters the lobes in a process that is similar to the one that operates during southward IMF.

1 Introduction

It has long been established that reconnection at Earth's magnetopause is the primary driver for magnetospheric plasma convection. The most important parameter controlling reconnection is the orientation of

the interplanetary magnetic field (IMF). For southward IMF reconnection occurs at the dayside magnetopause and drives the well-known two-cell convection pattern. If a B_y component is present in the IMF the dayside reconnection topology changes either into a "split separator" type [*Crooker*, 1986] or into a configuration in which the merging X-line runs across the subsolar point at an angle. For northward IMF merging is thought to occur poleward of the cusps between IMF and lobe field lines [*Dungey*, 1963]. There is now increasing evidence that this type of merging indeed occurs [*Omelchenko et al.*, 1983; *Kessel et al.*, 1996; *Berchem et al.*, 1995a, b; *Song and Russell*, 1992; *Le et al.*, 1996]. These observations mostly pertain to situations where the IMF is almost due northward. If a substantial B_y component is present in the IMF the reconnection site is expected to move from just poleward of the cusp to the tail flanks [*Crooker*, 1986]. Indeed, Gosling et al. [1991; 1996] observed reconnection signatures in the flanks of the magnetopause using ISEE data.

While the reconnection driven convection patterns for southward IMF are clearly established and well understood, the patterns for northward IMF are less clear. In general, ionospheric convection is found to be sunward over the pole with a four cell pattern during strongly northward IMF [*Reiff*, 1982]. The situation is different, however, when a substantial IMF B_y component is present. In that case, the convection pattern often consists of two or three cells, such that the dominating cell is situated over the magnetic pole [*Reiff and Burch*, 1985]. This cell, which is often called the "lobe cell", then likely maps entirely to the tail lobes [*Hill*, 1994]. Although the mapping of lobe cells appears to be obvious, it is not clear what drives the lobe convection in this situation. Of particular concern is the fact that in a steady state situation sunward convection in the ionosphere would map to anti-sunward convection in the tail, which seems to be dynamically impossible. Because the lobe is rarely observed by spacecraft and because measuring plasma velocities in the tenuous lobes is difficult no direct *in-situ* observations of lobe convection during northward IMF conditions have yet been presented.

In this paper we use observation of the Interball tail probe in conjunction with global simulations of Earth's magnetosphere and ionosphere to study an event in which we observe both reconnection at the tail flank and the consequences of the associated lobe convection. In section 2 we describe the instruments and the observations. In section 3 we describe the model and present the simulation results. Finally, in section 4 we summarize and discuss our results.

2 Observations

The event of interest occurred on October 19, 1995, 1300-1700UT. The Wind spacecraft monitored the solar wind and IMF upstream of Earth's bow shock, located near (175,-2,-13) R_E in GSE coordinates. At the same time the Interball tail probe was located near (-23,-16,11) R_E in GSE coordinates and near (-23,-10,17) R_E in GSM coordinates at the tail boundary.

2.1 Solar wind

Figure 1 shows the solar wind parameters in GSM coordinates as obtained from the Wind spacecraft. The IMF is fairly steady during the interval. B_x is small, B_z is positive at about 15nT, B_y is negative and of similar magnitude. The velocity and temperature have typical values of the slow solar wind, i.e., 400 km/s and 2-4 eV, respectively. The solar wind density increases from about 5 cm^{-3} at the beginning of the interval to values of about 20 cm^{-3} toward the end of the interval. Thus the solar wind dynamic pressure is elevated over typical values by a factor of 2-4 during most of the interval. For this reason the

magnetosphere and the magnetotail are somewhat compressed, causing Interball to stay in the vicinity of the tail magnetopause for an extended interval.

2.2 Interball

The Interball tail probe was launched on August 3, 1995 to study the plasma and field environment of Earth's magnetosphere and geomagnetic tail. The initial spacecraft's orbit of 1.01 by 31 R_E is inclined by about 90° with respect to the ecliptic, thus the spacecraft samples the high latitude tail once per year. In this study we use plasma data from the SCA-1 plasma analyzer [*Vaisberg et al.*, 1995, 1997] and magnetic field data from the MIF magnetometer [*Klimov et al.*, 1995, 1997]. The magnetometer samples the three magnetic field components at a frequency of 1 Hz. The SCA-1 plasma analyzer samples a full three dimensional spectrum in the energy range from 50 eV to 5 keV every 10 seconds. From the particle spectra the plasma moments density, velocity, and temperature are computed and used in this study.

On October 19, 1995, 1300-1700UT, the Interball tail probe was located near (-23,-16,11) R_E in GSE coordinates and the near (-23,-10,17) R_E in GSM coordinates. Figure 2 shows SCA-1 energy-time spectra from 8 directions along cones of 2°, 17°, 40°, 65°, 115°, 140°, 163°, and 178° from the nearly sunward axis of the satellite's rotation.

There are basically two types of plasma observed. At times the entire plasma distribution is tailward flowing and no plasma is observed by the tailward looking detectors. We interpret this plasma population as magnetosheath plasma. Within two prominent intervals, from 1501 to 1515 UT and from 1550 to 1711 UT less dense plasma is observed with the flow direction changing from sunward to anti-sunward. We interpret these intervals as Interball being in the tail lobes. Very dilute lobe plasma was also observed before the magnetopause crossing at 1330 UT. Thus, relatively dense plasma convected to the tail lobe during the 1330 to 1501 UT interval.

Figure 3 shows the magnetic field and the plasma moments. Times when Interball is in the lobes are shaded. At these times the x-component of the velocity varies in a characteristic way. At three magnetopause crossings, at 1515 UT, 1555 UT, and 1711 UT a thin layer of anti-sunward moving hot magnetospheric plasma was observed before the satellite enters the sunward-flowing plasma layer. At 1501 UT the satellite entered from the magnetosheath directly into sunward moving hot magnetospheric plasma. There is another time interval, 1612 to 1640 UT, when lobe plasma is moving anti-sunward. When Interball is in the magnetosheath the flow is nearly steady in the anti-sunward direction and the flow velocity is close to the solar wind speed, as expected.

The transition between the lobe and the magnetosheath intervals are also marked by sharp rotations of the magnetic field, giving further evidence that Interball indeed crosses the tail magnetopause. The density and temperature values are also consistent with this picture. In the magnetosheath the density is high with values of about 4 cm^{-3}, and the temperature is low with values of a few hundred eV. By contrast, the lobe temperatures are higher (about 1 keV) and the densities are significantly lower (0.03-0.2 cm^{-3}). One should note, however, that both the density and temperature are underestimated by the SCA-1 instrument because of its limited energy range.

Another salient feature of these observations is the velocity enhancement that is observed at each of the boundary crossings. These enhancements always occur on the magnetosheath side of the boundary and are seen in all three velocity components. At some crossings, most notably at 1330 UT, the V_x component is enhanced to values that are larger than the ambient magnetosheath flow. At other crossings there are strong deflections of the flow in the y and x directions. We interpret these flow features as sig-

natures of reconnection. Because the flow is accelerated above the ambient magnetosheath flow velocity the X-line must lie earthward of Interball. We have inspected the detailed three-dimensional distribution functions in the vicinity of the boundary crossings and found that they are D-shaped and consistent with this reconnection picture. A more thorough analysis of the reconnection signatures will be published elsewhere.

Also important for this study is the gradual increase of the lobe density during this event. Each of the three major lobe intervals shows higher densities than the previous one. Apparently, the lobe is slowly filling with plasma during this interval. From the single spacecraft Interball observations it is virtually impossible to determine where this plasma comes from. In general, one would not expect plasma entering the lobes under northward IMF conditions, but rather under southward IMF conditions [*Gosling et al.*, 1984, 1985; *Siscoe and Sanchez*, 1987; *Sanchez et al.*, 1990]. As we shall show below with our simulation results below, the appearance of this plasma can be explained by lobe circulation which is driven by lobe - IMF reconnection.

3 Simulation

We use a global MHD code which includes an ionospheric model for the closure of field-aligned currents [*Raeder et al.*, 1997, 1998; *Raeder*, 1999]. In order to accommodate the large simulation volume with a long tail and long simulation times the simulation code was parallelized for running on Multiple Instruction-Multiple Data (MIMD) machines by using a domain decomposition technique [*Fox et al.*, 1988]. The model solves the ideal MHD equations (modified as described below) for the magnetosphere and a potential equation for the ionosphere. Numerical effects, such as diffusion, viscosity, and resistivity, are necessarily introduced by the numerical methods. These permit viscous interactions and to a limited extent magnetic field reconnection. For this study we keep an explicit resistivity term in Ohm's law, which is discussed in more detail below.

3.1 Outer magnetosphere

The magnetospheric (MHD) part of the model is solved using a finite difference method which is conservative for the gas-dynamic part of the MHD equations:

$$\frac{\partial \rho}{\partial t} = -\nabla \cdot (\rho \mathbf{v}) \tag{1}$$

$$\frac{\partial \rho \mathbf{v}}{\partial t} = -\nabla \cdot (\rho \mathbf{v}\mathbf{v} + p\mathsf{I}) + \mathbf{j}\times\mathbf{B} \tag{2}$$

$$\frac{\partial e}{\partial t} = -\nabla \cdot (\{e + p\}\mathbf{v}) + \mathbf{j} \cdot \mathbf{E} \tag{3}$$

$$\frac{\partial \mathbf{B}}{\partial t} = -\nabla\times\mathbf{E} \tag{4}$$

$$\nabla \cdot \mathbf{B} = 0 \tag{5}$$

$$\mathbf{E} = -\mathbf{v}\times\mathbf{B} + \eta\mathbf{j} \tag{6}$$

$$\mathbf{j} = \nabla\times\mathbf{B} \tag{7}$$

$$e = \frac{1}{2}\rho v^2 + \frac{p}{\gamma - 1} \tag{8}$$

where ρ is the plasma density, $\mathbf{v}$ the velocity, p the plasma pressure, I the unit tensor of rank 3, e the plasma energy density, γ the specific heat ratio (a value of 5/3 is used in these simulations), $\mathbf{B}$ the magnetic field, $\mathbf{j}$ the current density, $\mathbf{E}$ the electric field, and η the electrical resistivity. Note that all variables are normalized to reference values in order to eliminate numerical factors such as the permeability of free space.

The $\mathbf{j}\times\mathbf{B}$ and $\mathbf{E}\cdot\mathbf{j}$ terms are treated as source terms because the very low plasma β and the large magnetic field gradients near the Earth do not allow the use of the full conservative form of the MHD equations. The electrical resistivity η is given by a model of anomalous resistivity:

$$\eta = \alpha j'^2 \quad \text{if} \quad j' \geq \delta, \quad 0 \text{ otherwise} \tag{9}$$

$$j' = \frac{|j|\Delta}{|B| + \epsilon} \tag{10}$$

where j is the local current density, B the local magnetic field, Δ is the grid spacing, and ϵ is a very small number (10^{-8}) introduced to avoid dividing by zero. The normalized current density j' ($0 \leq j' \leq 1$) is used as a switch for the resistivity. In places where the resistivity is switched on it becomes proportional to the square of the local current density. Similar resistivity models have been used in the past to model the kinetic effects that lead to anomalous resistivity [*Sato and Hayashi*, 1979; *Hoshino*, 1991]. The parameters α and δ determine the value of the resistivity and the current density threshold that must be reached for the resistivity to be switched on. The parameter δ (δ=0.75 in these simulations) is chosen such that the resistivity η is nonzero only at a very few gridpoints in strong current sheets. The dimensionless parameter α has a value of 0.03 for the simulations shown in this paper. With this choice of α the largest possible value for η is η_{max}=2×10$^6\Omega$m. Because η depends on the local plasma parameters its value varies strongly both in time and space. Typically, at any given time only a few tens to a few hundreds grid cells (out of about 10^6) reach values larger than one tenth of η_{max}.

The numerical grid is rectangular and nonuniform with the highest spatial resolution (about 0.5 R_E) near Earth. It extends 20 R_E in the sunward direction, 400 R_E in the tailward direction and $\pm$50 R_E in the Y and Z directions. The gas-dynamic part of the equations is spatially differenced by using a technique in which fourth order fluxes are hybridized with first order (Rusanov) fluxes [*Harten and Zwas*, 1972; *Hirsch*, 1990]. The magnetic induction equation is treated somewhat differently [*Evans and Hawley*, 1988] in order to conserve $\nabla\cdot\mathbf{B} = 0$ exactly. The numerical fluxes for Faraday's equation are based on Van Leer's second order flux limited upwind scheme [*Van Leer*, 1977]. The time stepping scheme for all variables consists of a low order predictor with a time centered corrector, which is accurate to the second order in time. Thus, the code is globally of fourth order spatial accuracy in the gas dynamic variables (density, momentum, and energy density), of second order spatial accuracy in the magnetic field components, and of second order accuracy in the time differencing.

The outer boundary conditions are fixed at the given solar wind values on the upstream side. At the other boundaries we apply open, i.e., zero normal derivative, boundary conditions.

3.2 Ionosphere

The inner boundary, where the MHD quantities are connected to the ionosphere, is taken to be a shell of radius 3.7 R_E centered at Earth. The choice of this radius is a compromise necessitated by numerical considerations, such as very high Alfvén speeds and very large magnetic field gradients closer to the

Earth. However, this choice allows for the proper mapping of all relevant field-aligned current (FAC) systems down to about 59^o magnetic latitude. The placement of the inner boundary, together with the lack of gradient and curvature drift terms in the MHD equations, also inhibits the formation of a ring current. Inside this shell we do not solve the MHD equations, but assume a static dipole field. The important physical processes earthward of that shell are the flow of FACs and the closure of these currents in the ionosphere. Every few time steps (corresponding to a time interval of less than 5 s in real time) we use the static dipole field to map the magnetospheric FACs from the 3.7 R_E shell onto the polar cap. We then use the FACs as input for the ionospheric potential equation:

$$\nabla \cdot \Sigma \cdot \nabla \Phi = -j_{\parallel} \sin I \tag{11}$$

which is solved on the surface of a sphere with a radius of 1.015 R_E. Here Φ denotes the ionospheric potential as a function of magnetic latitude and local time, Σ is the tensor of the ionospheric conductance, $j_{\parallel}$ is the mapped FAC with the downward current considered positive and corrected for flux tube convergence, and I is the inclination of the dipole field at the ionosphere. The boundary condition Φ = 0 is applied at the equator.

For the ionospheric Hall and Pedersen conductances, Σ_H and Σ_P, which enter the conductance tensor Σ [*Kamide and Matsushita*, 1979], three ionization sources are taken into account. First, for the solar EUV ionization we use an empirical model [*Moen and Brekke*, 1993] that depends only on the solar 10.7 cm flux ($F_{10.7}$) and the solar zenith angle (χ):

$$\Sigma_H = (F_{10.7})^{0.53}(0.81k + 0.54k^{1/2}) \tag{12}$$

$$\Sigma_P = (F_{10.7})^{0.49}(0.34k + 0.93k^{1/2}) \tag{13}$$

$$k = \cos\chi \tag{14}$$

Second, we compute the mean energy E_0 and energy flux F_E of precipitating electrons that are accelerated by a parallel potential drop $\Delta\Phi_{\parallel}$ in regions of upward field-aligned currents [*Knight*, 1972; *Lyons et al.*, 1979]:

$$F_E = \Delta\Phi_{\parallel}|j_{\parallel}| \tag{15}$$

$$E_0 = e\Delta\Phi_{\parallel} \tag{16}$$

$$\Delta\Phi_{\parallel} = \frac{e^2 n_e}{\sqrt{2\pi m_e k T_e}} \max(0, -j_{\parallel}) \tag{17}$$

Third, diffuse electron precipitation is modeled by assuming complete pitch angle scattering of electrons at 3.7 R_E [*Kennel and Petschek*, 1966]:

$$F_E = n_e(kT_e/2\pi m_e)^{\frac{1}{2}} \tag{18}$$

$$E_0 = kT_e \tag{19}$$

in which n_e, T_e, and m_e are the electron density, temperature, and mass, respectively, taken at the 3.7 R_E shell. The conductances are then computed from the electron precipitation parameters using the empirical relation [*Robinson et al.*, 1987]:

$$\Sigma_P = [40E_0/(16 + E_0^2)]F_E^{1/2} \tag{20}$$

$$\Sigma_H = 0.45E_0^{5/8}\Sigma_P \tag{21}$$

Using the mapped FACs and ionospheric conductances, the potential equation is solved using a pseudo spectral Galerkin method [*Canuto et al.*, 1987], and the ionospheric potential is mapped to the 3.7 R_E shell where it is used as a boundary condition for the magnetospheric flow by taking $\mathbf{v} = (-\nabla\Phi)\times\mathbf{B}/B^2$.

3.3 Initial conditions

The initial conditions for the magnetic field are constructed from the superposition of the Earth's dipole over an equally strong mirror dipole, such that B_x vanishes at x = 16 R_E. Sunward of the plane of symmetry at 16 R_E the field is replaced by the initial solar wind field. This procedure ensures a divergence-free transition from the constant solar wind field to the magnetospheric field. The simulation box is initially filled with tenuous (0.1 cm^{-3}) and cold (5000 K) plasma of zero velocity. The simulation run is started at 0800 UT with a southward IMF in order to let the unphysical initial conditions evolve into a magnetospheric configuration. After two hours (at 1000 UT) we start using ballistically propagated Wind data as input to the simulation. Thus, the period of interest, 1200 to 1800 UT begins 4 hours after the start of the simulation; at that time effects of the initial conditions should no longer play any role.

3.4 Model - data comparison

In order to compare the simulation results with the Interball data we take time series at the Interball location in the simulation box and plot these together with the data. Figure 4 shows such a comparison. From top to bottom the magnetic field components, the field elevation angle ($\mathtt{asin}(B_z/B)$), the field clock angle ($\mathtt{atan}(B_b/B_z)$), the total field, the x-component of the velocity, the plasma density, and the plasma pressure are shown for both Interball (in red) and the simulation (black curves). There is in general a reasonable agreement between the data and the simulation results. Of course, there no one to one match, mainly because of the limited resolution of the simulation and because Interball is always located very close to the magnetopause where small positional changes can have a dramatic effect on the observed fields and plasma moments. In particular, smaller scale features of the order of a few minutes are missing from the simulation. However, the simulation captures many of the main features. The first boundary crossing at around 1330 UT is clearly visible in the B_y and B_z components as well as in the plasma parameters. There are also clear enhancements of the flow V_x component on the magnetosheath side. The plasma density and pressure are generally somewhat larger than the observed values, which may in part be due to the limited energy range of the plasma instrument. Also, the $|V_x|$ values are generally larger in the simulation as compared to the Interball measurements, however, the measured values are also smaller than the ambient solar wind values, which may point in part to an instrument effect. The trend of increasing density in the tail lobe during this interval is evident both in the data and in the model results. Because of these favorable comparisons we are confident that the model gives a fair representation of the magnetosphere at this time, including all the relevant physical processes.

3.5 Reconnection geometry

Figure 5 shows a three-dimensional rendering of the simulated magnetosphere viewed from a sunward-dawnward-northward perspective at 1400 UT. The equatorial plane shows color coded the plasma pressure, with magenta depicting low values, green and yellow depicting intermediate values, and red depicting high values. The bow shock, magnetosheath, magnetopause, and plasma sheet are clearly visible

and provide guidance in this figure. The noon-midnight meridian and the plane at X=-23.1 R_E show color coded the plasma velocity with the same color scale. A set of blue field lines starts at 66° magnetic latitude and helps to illustrate the orientation of Earth's dipole. The blue spherical surface at the center is the inner boundary of the simulation domain 3.5 R_E from Earth. The small blue sphere in the X=-23.1 R_E plane indicates the Interball position. The green colored field line passes through the spacecraft. The set of pink field lines is chosen such that they all pass through the X=-23.1 R_E plane at the Interball Y position, but at different Z values.

From the green field line it is obvious that Interball is at this time located just outside of the lobe in the magnetosheath. This field line has a strong kink sunward of Interball which indicates that it has formed by reconnection between the lobe field and the IMF somewhat earlier. The set of pink field lines confirms this picture. Field lines that pass just below Interball have their kink located closer to Earth, whereas field lines that pass further below Interball connect to Earth. The region just around the sharp kink of the earth most unconnected field line and the open field line of highest latitude is the reconnection site. It is located at about (-3,-12,9) R_E in GSE coordinates, i.e., at (-3,-6.5,13.5) R_E in GSM coordinates. The kinked field lines emanating tailward from the reconnection site exert tailward acceleration on the plasma. This acceleration is clearly visible in the plane at X=-23.1 which shows the color coded velocity. Just outside of the magnetopause, and in the vicinity of Interball, there is a layer of fast flowing plasma (red and yellow) whose velocity exceeds the velocity of the solar wind and the velocity in the surrounding magnetosheath. The thickness of this high velocity layer is about two to four R_E , and it is about 15 to 20 R_E wide. There is also a more extended region of flows at higher latitudes that are less accelerated than those downstream of the reconnection but still faster than the solar wind. These flows appear to be accelerated by IMF field lines that have draped over the magnetosphere, and which also exert a tailward force on the plasma. Such accelerated flows have been reported previously by *Chen et al.* [1993].

We have inspected the size of the reconnection region and found that it is of very limited extent, roughly 2 R_E in the Y direction and about 4 R_E in the X direction. We have also examined the location and size of the reconnection region as a function of time during this interval. We found that neither its size nor its location changes significantly between 1200 and 1800 UT, which is consistent with the IMF data that also show very little variation during this interval.

3.6 Lobe convection

Figure 6 shows cuts of different quantities and at different times in the Y-Z plane at the Interball location, i.e., at X=-23.1 R_E. The left panels show the plasma density, the middle panels show color coded the X component of the plasma velocity (V_x) and the (V_y,V_z) components as arrows, and the right panels show the color coded current density. The snapshots are taken, from top to bottom, at 1330, 1500, and 1630 UT. The black crosses mark the Interball position in all of these figures.

From the strong density gradient and from the current density it is obvious that Interball is in the immediate vicinity of the magnetopause at all times. From the scale of the density gradient and from the width of the magnetopause current layer it is clear that the simulation severely under-resolves these features. For example, the current layer is about 1 R_E thick in these simulations, whereas the observed thickness is about one order of magnitude less [*Berchem and Russell*, 1982]. Thus, the rather smooth time series obtained from the simulation (see Figure 4) can be easily explained by the lack of resolution.

From the density plots it can be seen that the lobes slowly fill with plasma during this event. Although

it appears from the density plots that the lobes are getting compressed by the increasing solar wind density, this effect seems to be minor (compare with the current density plots on the right). Rather, there appears to be plasma entering the tail from the flanks. This effect is most pronounced by the tongue of plasma that emerges from the high latitude dusk side and extends in time more and more toward dawn and the Interball position at the dawn side magnetopause. The plasma entry is obviously driven by convective flows, which are shown in the middle panels. There is a steady dawnward flow in the tail toward the magnetopause in the vicinity of Interball. A similar, albeit weaker flow toward the magnetopause occurs in the southern dusk hemisphere of the tail. These flows are quite obviously driven by reconnection. The reconnection process described earlier at the tail flank continuously strips magnetic flux away from the tail which then convects tailward. This flux is then replaced by the flows that are observed here. The net magnetic flux of the tail does not change significantly, because for each flux tube that is stripped off the tail a new open flux tube is created, which initially drapes over the dayside magnetosphere [*Russell*, 1972; *Cowley*, 1983]. These overdraped field lines (see green flux tubes in Figure 5) eventually convect around the magnetosphere and are added to the lobes.

3.7 Ionospheric convection

Figure 7 shows in the upper panel the ionospheric convection pattern in the northern hemisphere at 1500 UT. The ionospheric potential is color coded (negative values are blue and positive values are yellow or red), and contours at 10 kV intervals are also drawn. Note that the contours are also streamlines of the ionospheric plasma flow. The green line shows the polar cap boundary, i.e., the boundary between open and closed field lines. The magnetic footpoint of Interball, which is at this time located in the lobe (see Figure 5), is marked by the black cross.

The convection pattern is comprised of two major cells. One cell is situated over the magnetic pole circulating counter-clockwise. This cell is commonly called the "lobe cell" [*Crooker*, 1992; *Hill*, 1994]. The second cell is kidney shaped and extends at lower latitudes, between 70° and 80° magnetic latitude, and between 18 and 24 hours magnetic local time. This cell circulates clockwise.

We have no observational convection pattern available for this interval. However several studies have addressed convection patterns for very similar IMF conditions. For example, *Lyons et al.* [1996,1998] present patterns for northward B_z, negative B_y conditions (their Figure 5), as well as *Lu et al.* [1994] (their Figure 5), *Knipp* [1993] (their Figures 3 and 5), and *Burke et al.* [1994] (their Figure 6, which should be flipped about the noon-midnight meridian because the IMF B_y is positive). These observational convection patterns are all very similar to the one in Figure 7, and the differences should be mainly due to the somewhat different IMF conditions and seasonal effects. Also, several models [*Reiff and Burch*, 1985; *Crooker*, 1992; *Crooker et al.*, 1998] predict a two cell structure like the one in Figure 7.

Although the convection patterns for northward IMF in the presence of an IMF B_y component are fairly well established from observations and by geometrical models, it is much less clear how they map to the tail. This simulation gives some clues as to this mapping. The lower panel of Figure 7 shows the ionospheric convection pattern mapped to the Y_{GSE} - Z_{GSE} plane through Interball. As expected, there is nearly a one to one correspondence between the mapped ionospheric convection pattern in Figure 7 and the tail convection pattern of Figure 6 (middle row and middle column). Thus, the plasma arriving at Interball comes from the dusk side of the tail, where new open field lines that have formed through lobe-IMF reconnection enter the tail. A bundle of such field lines can be seen in Figure 5 (the green field lines at high latitude). Just after these field lines form through lobe-IMF reconnection they drape over

the dayside magnetosphere. They are then swept along the dusk flank of the magnetosphere and enter the mid tail at the duskward "appendix" seen in the lower panel of Figure 7. Clearly, these field lines are of solar wind/magnetosheath origin and thus carry plasma that is of much higher density than commonly found in the lobes. Because this plasma must convect across the entire tail to reach the Interball position, a significant delay (several hours) between the lobe-IMF reconnection onset and the appearance of this plasma at Interball is expected, and indeed observed. This process of filling the lobes with plasma from the solar wind is very similar to the one observed during southward IMF [*Gosling et al.*, 1984, 1985]. In the latter case, the plasma enters the tail at high latitudes through the mantle, whereas in the northward IMF case like this the plasma takes a "detour" along the dayside and flank magnetopause via the overdraped field. There is also the possibility that a slow mode expansion fan forms, similar to what is predicted and observed for southward IMF [*Rosenbauer et al.*, 1975; *Gosling et al.*, 1984; *Siscoe and Sanchez*, 1987; *Sanchez et al.*, 1990]. However, because of the more complicated geometry in the northward IMF case this may be much more difficult to show either experimentally or via simulations.

Another interesting feature is the mapping of the lobe boundary between the tail and the ionosphere. We have traced magnetic field lines from points just inside of the magnetopause into the ionosphere. Each trace is marked in the Y_{GSE} - Z_{GSE} plane and the in the ionosphere plot of Figure 7 with a distinct color. This mapping is expected to be a continuous and smooth function, which the continuous color variation along the curve defined by these dots indeed shows. However, the mapping appears to be strongly irregular as the spacing of the dots in the ionosphere shows. Also, the dots should all lie on the green line which was computed by tracing field lines from the ionosphere into the magnetosphere. Although this holds by and large, there are some significant differences.

First, there is an extreme stretching of the mapping between 1600 and 2300 magnetic local time in the ionosphere. Thus, all field lines in this sector of the ionosphere and just poleward of the open-closed boundary map to essentially one point in the tail, namely the southern tip of dusk "appendix" of the northern lobe. Because many flow lines cut through the open-closed boundary in this sector of the ionosphere, there is a strong bunching of flow lines at the corresponding tail site. It also implies that this site is the primary entry site of plasma into the tail. Comparing the lower panel of Figure 7 with Figure 5 it is easy to see that this must be the site where the reconnected, overdraped field enters the tail lobes. Because the layer of overdraped field is rather thin ($\lesssim 1\ R_E$, near the limit of the resolution of the model) the entry site must also be of small extent.

Second, there is a near-singularity of the opposite kind in the mapping near the cusp. Essentially the entire magnetopause of the northern lobe at X_{GSE}=-23.1 R_E maps to a narrow throat near local noon. This throat extends from the cusp location to the center of the lobe convection cell and cuts the lobe convection cell open in such a way that the center of the convection cell does not map into the tail. If the center of the convection cell does not map into the tail, it must map on closed field lines. However, there are no closed field lines present anywhere near the mapping of the throat into the tail, which runs from about the Interball position to the tip of the dusk "appendix" (the magenta dots). Thus the field line mapping is singular in the vicinity of the throat. Because of the finite resolution of the simulation and the near-singular mapping it may well be possible that the throat has zero width in reality, i.e., that a singular line is running from the cusp to the center of the cell. If this is the case, then particle precipitation on either side of this line should be different and the singularity may be observable in precipitation data.

This particular mapping of the lobe cell may also solve a long-standing problem regarding the mapping of lobe cells in a steady state situation. *Hill* [1994] and *Vasyliunas* [1988] have pointed out that it is difficult to explain how anti-sunward magnetosheath flow can produce sunward flow in the ionosphere on

the same field line. In particular, they are concerned with the mapping of the lobe cell center that would have to map to a stagnation point in the solar wind, which seems not very plausible. Considering the singular or near-singular mapping found in this study the problem solves itself because the cell center maps nowhere (in a strict mathematical sense) or to closed field lines in a way that is still undefined. That would still leave the problem of sunward flow on anti-sunward convecting field lines. Here, the flaw Hill's and Vasyliunas's argument may be the assumption of steady state mapping over large distances into the tail. Because the flows on lobe field lines eventually become supermagnetosonic tailward (usually at a distance of about 150-200 R_E from Earth), the dynamics of the tailward portion of a field line becomes decoupled from its ionospheric end. In other words, the ionospheric end of the field line cannot know what the tailward end does, because no information can travel against the superfast tailward flow.

3.8 Tail convection animation

Because the reconnection process and the convection of solar wind plasma into the tail is an intrinsically time dependent process we have produced an animation from the simulation that provides better insight. The animation is shown in Movie 1 (see "Electronic Supplements" on the journals' homepage at `http://www.elsevier.com/locate/jastp` or *http://www.elsevier.nl/locate/jastp*). The animation frames are three-dimensional renderings of the magnetosphere that are very similar to Figure 5. The X_{GSE}=-23.1, Y_{GSE}=0, and Z_{GSE}=0, show color coded the plasma number density, on a logarithmic scale ranging from 0.1cm^{-3}(blue) to 30cm^{-3}(red). The Interball position is marked by the small sphere in the X_{GSE}=-23.1 plane, and the field line passing through Interball is drawn in green. The magenta field lines start in the magnetic noon-midnight meridian.

The animation shows clearly the overdraping of reconnected field lines over the dayside magnetosphere and their convection into the dusk hemisphere. Here, they are added to the lobes, as already shown in the previous section. With these new field lines, plasma from the magnetosheath is entering the northern lobe. This plasma convects slowly across the lobe from dusk to dawn. Some of that plasma eventually reaches the Interball position which explains the Interball observation of slowly increasing lobe plasma density through this event.

4 Summary and discussion

In this study we have presented Interball observations from the high latitude mid-tail magnetopause that provide further evidence that reconnection between the IMF and lobe field lines occurs during periods of northward IMF. The event studied here is somewhat different from previous studies of the same process [*Omelchenko et al.*, 1983; *Gosling et al.*, 1991, 1996; *Kessel et al.*, 1996; *Berchem et al.*, 1995a, b; *Le et al.*, 1996] because Interball is located well tailward of the reconnection site, yet still observes distinct reconnection signatures, such as accelerated flows and D-shaped distribution functions. This event is also distinct in that the IMF and solar wind is fairly steady for a six hour period. This allows Interball to observe a convection feature in the tail that takes several hours to develop, namely the slow filling of the tail lobes with plasma of solar wind origin.

These Interball observations provide an important benchmark for our simulation of this event. The simulation reproduces the key Interball observations, namely the accelerated flows, the boundary crossings, and the increasing plasma density of the lobes at least qualitatively, and in part also quantitatively.

The simulation also produces a ionospheric convection pattern that is consistent with previous observations of ionospheric convection under similar IMF conditions. This allows us to use the simulation results to extend Interball's view globally and to analyze the processes in more detail.

The simulation confirms that reconnection between lobe and IMF field lines occurs throughout the entire interval. The reconnection site is found to lie near the terminator where the lobe field and the draped IMF is anti-parallel. The reconnection site is also found to be of small extent (about $2R_E$), and varies little through the interval. Because of the finite IMF B_y IMF field lines do not reconnect simultaneously in both hemispheres as first proposed by *Russell* [1972], but form new open field lines that drape over the dayside magnetosphere. These newly formed field lines then convect over the magnetosphere's flanks and are added to the tail lobes. This process results in no net change of lobe flux, because on lobe flux tube is replaced by another lobe flux tube.

Mapping of the lobe boundary from the Interball position near X_{GSE}=-23.1 R_E into the ionosphere reveals two singularities. First, there is a very small area of the lobe where reconnected flux tubes enter the tail (the "entry window") that maps to an extended area in the ionosphere, spanning there about 6 hours of magnetic local time. Second, a mapping throat forms from the cusp to the center of the ionospheric lobe cell, that maps to essentially the entire northern lobe magnetopause. Because of this throat, or singular line, the lobe cell is cut open, and the center of the lobe cell cannot map into the lobe. This resolves the mapping problem raised by *Vasyliunas* [1988] and *Hill* [1994] who have argued that mapping the lobe cell center (a stagnation point) to a tailward convecting field line is dynamically impossible.

The existence of singularities in the magnetic mapping between the ionosphere and the tail needs to be taken into account when studying the coupling between the ionosphere and the tail using empirical or theoretical magnetic field models [e.g., *Pulkkinen et al.*, 1991; *Elphinstone et al.*, 1991; *Elphinstone and Hearn*, 1992]. As our results show, singularities can arise for benign solar wind conditions and in near steady state situations. Thus singularities appear to be even more likely when the magnetotail undergoes a rapid re-configuration, such as during substorms or storms [see also: *Hesse et al.*, 1997]. Because most empirical magnetic field models [*Tsyganenko*, 1990; *Tsyganenko et al.*, 1998] describe the Earth's field in terms of smooth functions important aspects of the mapping relationships may be missed.

Finally, the "entry window" that is opened up by lobe - IMF reconnection –not at the reconnection site, but almost opposite to it– allows not only magnetic flux to enter the tail, but also plasma of solar wind origin. This plasma slowly convects through the tail lobe in a fashion similar to the one previously established for southward IMF conditions [*Gosling et al.*, 1984, 1985; *Siscoe and Sanchez*, 1987; *Sanchez et al.*, 1990]. For northward IMF, however, the polarity of the filling process is opposite: A negative B_y will first cause the northern dawn and southern dusk lobes to be filled with plasma. The prevailing convection pattern from the "entry window" toward the reconnection site, however, will fill the entire tail lobes with plasma eventually. The time scale for this process is several hours, as both the simulation and the Interball observations show.

Acknowledgments:

The authors thank S. Klimov and N. Rybyeva for providing the Interball MIF magnetic field data and R. Lepping and K. Ogilvie for providing the Wind magnetic field and plasma data, respectively. This work was supported by NSF grants ATM 97-13449 and ATM 98-01937 at UCLA. The work of one of the authors (O. Vaisberg) was supported by NRC grant NASW-99027. V. Smirnov and L. Avanov were partly supported through NASA grant NAG5-4130. Computations were performed on the IBM SP-2 of the San Diego Supercomputer Center and the NSCA Origin2000. IGPP publication 5424.

References

Berchem, J., and C. T. Russell, The thickness of the magnetopause current layers: ISEE 1 and 2 observations, *J. Geophys. Res.*, *87*, 2108, 1982.

Berchem, J., J. Raeder, and M. Ashour-Abdalla, Reconnection at the magnetospheric boundary: Results from global MHD simulations, in *Physics of the Magnetopause*, edited by B. U. Sonnerup and P. Song, vol. 90 of *AGU Geophysical Monograph*, p. 205, 1995a.

Berchem, J., J. Raeder, and M. Ashour-Abdalla, Magnetic flux ropes at the high-latitude magnetopause, *Geophys. Res. Lett.*, *22*, 1189, 1995b.

Burke, W. J., E. M. Basinska, N. C. Maynard, W. B. Hanson, J. A. Slavin, and J. D. Winningham, Polar cap potential distributions during periods of positive IMF b_y and b_z, *J. Atmos. Terr. Phys.*, *56*, 209, 1994.

Canuto, C., M. Y. Hussaini, A. Quarteroni, and T. A. Zang, *Spectral Methods in Fluid Dynamics*, Springer-Verlag, New York, 1987.

Chen, S. A., M. G. Kivelson, J. T. Gosling, R. J. Walker, and A. J. Lazarus, Anomalous aspects of magnetosheath flow and of the shape and oscillations of the during an interval of strongly northward Interplanetary Magnetic Field, *J. Geophys. Res.*, *98*, 5727, 1993.

Cowley, S. W. H., Interpretation of observed relations between solar wind characteristics and effects at ionospheric altitudes, in *High Latitude Space Plasma Physics*, edited by B. Hultquist and T. Hagfors, p. 225, New York, Plenum, 1983.

Crooker, N. U., Global geometry of merging at the dayside magnetopause, in *Solar Wind - Magnetosphere Coupling*, edited by Y. Kamide and J. A. Slavin, p. 287, Terra Scientific Publishing Company, 1986.

Crooker, N. U., Reverse convection, *J. Geophys. Res.*, *97*, 19,363, 1992.

Crooker, N. U., J. G. Lyon, and J. A. J. A. Fedder, MHD model merging with IMF B_y: Lobe cells, sunward polar cap convection, and overdraped lobes, *J. Geophys. Res.*, *103*, 9143, 1998.

Dungey, J. W., The structure of the exosphere or adventures in velocity space, in *Geophysics, The Earth's Environment*, edited by C. DeWitt, J. Hieblot, and A. Lebeau, p. 550, Newark, N.J., Gordon and Breach, 1963.

Elphinstone, R. D., and D. Hearn, Mapping of the auroral distribution during quiet times and substorm recovery, in *Substorms I*, vol. ESA SP-335, p. 13, Paris, 1992.

Elphinstone, R. D., D. Hearns, J. S. Murphree, and L. L. Cogger, Mapping using the Tsyganenko long magnetospheric model and its relationship to Viking auroral images, *J. Geophys. Res.*, *96*, 1467, 1991.

Evans, C. R., and J. F. Hawley, Simulation of magnetohydrodynamic flows: A constrained transport method, *Astrophys. J.*, *332*, 659, 1988.

Fox, G. C., M. A. Johnson, G. A. Lyzenga, S. W. Otto, J. K. Salmon, and D. W. Walker, *Solving Problems on Concurrent Processors*, Prentice Hall, Englewood Cliffs, N.J., 1988.

Gosling, J. T., D. N. Baker, S. J. Bame, E. W. Hones, D. J. McComas, R. D. Zwickl, J. A. Slavin, E. J. Smith, and B. T. Tsurutani, Plasma entry into the distant tail lobes: ISEE 3, *Geophys. Res. Lett.*, *11*, 1078, 1984.

Gosling, J. T., D. N. Baker, J. J. Bame, W. C. Feldman, R. D. Zwickl, and E. J. Smith, North-south and dawn-dusk asymmetries in the distant tail lobes: ISEE 3, *J. Geophys. Res.*, *90*, 6354, 1985.

Gosling, J. T., M. F. Thomsen, S. J. Bame, and R. C. Elphic, Observations of reconnection of interplanetary and lobe magnetic field lines at the high-latitude magnetopause, *J. Geophys. Res.*, *96*, 14,097, 1991.

Gosling, J. T., M. F. Thomsen, G. Le, and C. T. Russell, Observations of magnetic reconnection at the lobe magnetopause, *J. Geophys. Res.*, *101*, 24,765, 1996.

Harten, A., and G. Zwas, Self-adjusting hybrid schemes for shock computations, *J. Comput. Phys.*, *9*, 568, 1972.

Hesse, M., J. Birn, and R. A. Hoffman, On the mapping of ionospheric convection into the magnetosphere, *J. Geophys. Res.*, *102*, 9543, 1997.

Hill, T. W., Theoretical models of polar-cap convection under the influence of a northward interplanetary magnetic field, *J. Atmos. Terr. Phys.*, *56*, 185, 1994.

Hirsch, C., *Numerical Computation of Internal and External Flow*, vol. II, John Wiley, New York, 1990.

Hoshino, M., Forced magnetic reconnection in a plasma sheet with localized resistivity profile excited by lower hybrid drift type instability, *J. Geophys. Res.*, *96*, 11,555, 1991.

Kamide, Y., and S. Matsushita, Simulation studies of ionospheric electric fields and currents in relation to field aligned currents, 1, quiet periods, *J. Geophys. Res.*, *84*, 4083, 1979.

Kennel, C. F., and H. E. Petschek, Limit on stably trapped particle fluxes, *J. Geophys. Res.*, *71*, 1, 1966.

Kessel, R. L., S.-H. Chen, J. L. Green, S. F. Fung, S. A. Boardsen, L. C. Tan, T. E. Eastman, J. D. Craven, and L. A. Frank, Evidence of high-latitude reconnection during northward IMF: Hawkeye observations, *Geophys. Res. Lett.*, *23*, 583, 1996.

Klimov, S., S. Romanov, E. Amata, and J. Blecki, Aspi experiment: Measurements of fields and waves onboard the Interball-Tail mission, in *INTERBALL Mission and Payload*, edited by dont know, vol. 12345, p. 120, 1995.

Klimov, S., et al., ASPI experiment: Measurements of fields and waves on board the INTERBALL-1 spacecraft, *Ann. Geophysicae*, *15*, 514, 1997.

Knight, S., Parallel electric fields, *Planet. Space Sci.*, *21*, 741, 1972.

Knipp, D. J., Ionospheric convection response to slow, strong variations in a northward interplanetary magnetic field: A case study for January 14, 1988, *J. Geophys. Res.*, *98*, 19,273, 1993.

Le, G., C. T. Russell, J. T. Gosling, and M. F. Thomsen, ISEE observations of low-latitude boundary layer for northward interplanetary magnetic field: Implications for cusp reconnection, *J. Geophys. Res.*, *101*, 27,239, 1996.

Lu, G., et al., Interhemispheric asymmetry of the high latitude convection pattern, *J. Geophys. Res.*, *99*, 6491, 1994.

Lyons, L. R., The Geospace Environment Modeling Grand Challenge, *J. Geophys. Res.*, *103*, 14,781, 1998.

Lyons, L. R., D. Evans, and R. Lundin, An observed relation between magnetic field aligned electric fields and downward electron energy fluxes in the vicinity of auroral forms, *J. Geophys. Res.*, *84*, 457, 1979.

Lyons, L. R., G. Lu, O. de la Beaujardiere, and F. J. Rich, Synoptic maps of polar caps for stable interplanetary magnetic field intervals during January 1992 Geospace Environment Modeling campaign, *J. Geophys. Res.*, *101*, 27,283, 1996.

Moen, J., and A. Brekke, The solar flux influence on quiet time conductances in the auroral ionosphere, *Geophys. Res. Lett.*, *20*, 971, 1993.

Omelchenko, A. N., O. L. Vaisberg, and C. T. Russell, Further analysis of plasma bursts in Earth's boundary layer at high latitudes, *Cosmic Research*, *21*, 687, 1983.

Pulkkinen, T. I., H. E. J. Koskinen, and R. J. Pellinen, Mapping of auroral arcs during substorm growth phase, *J. Geophys. Res.*, *96*, 21,087, 1991.

Raeder, J., Modeling the magnetosphere for northward interplanetary magnetic field: Effects of electrical resistivity, *J. Geophys. Res.*, *104*, 17,357, 1999.

Raeder, J., J. Berchem, and M. Ashour-Abdalla, The Geospace Environment Modeling grand challenge: Results from a Global Geospace Circulation Model, *J. Geophys. Res.*, *103*, 14,787, 1998.

Raeder, J., et al., Boundary layer formation in the magnetotail: Geotail observations and comparisons with a global MHD model, *Geophys. Res. Lett.*, *24*, 951, 1997.

Reiff, P. H., Sunward convection on both polar caps, *J. Geophys. Res.*, *87*, 5976, 1982.

Reiff, P. H., and J. L. Burch, B_y dependent dayside plasma flow and Birkeland currents in the dayside magnetosphere, 2, A global model for northward and for southward IMF, *J. Geophys. Res.*, *90*, 1595, 1985.

Robinson, R. M., R. R. Vondrak, K. Miller, T. Dabbs, and D. Hardy, On calculating ionospheric conductances from the flux and energy of precipitating electrons, *J. Geophys. Res.*, *92*, 2565, 1987.

Rosenbauer, H., H. Grunwaldt, M. D. Montgomery, G. Paschmann, and N. Sckopke, Heos 2 plasma observations in the distant polar magnetosphere: The plasma mantle, *J. Geophys. Res.*, *80*, 2723, 1975.

Russell, C. T., The configuration of the magnetosphere, in *Critical Problems of Magnetospheric Physics*, edited by E. R. Dyer, p. 1, Washington, D. C., Nat. Acad. of Sci., 1972.

Sanchez, E., G. L. Siscoe, J. T. Gosling, E. W. Hones, and R. P. Lepping, Observations of rotational discontinuity slow expansion fan structure of the magnetotail boundary, *J. Geophys. Res.*, *95*, 61, 1990.

Sato, T., and T. Hayashi, Externally driven magnetic reconnection as a powerful magnetic energy converter, *Phys. Fluids*, *22*, 1189, 1979.

Siscoe, G. L., and E. Sanchez, An MHD model for the complete open magnetotail boundary, *J. Geophys. Res.*, *92*, 7405, 1987.

Song, P., and C. T. Russell, Model of the formation of the low-latitude boundary layer for strongly northward interplanetary magnetic field, *J. Geophys. Res.*, *97*, 1411, 1992.

Tsyganenko, N. A., Quantitative models of the magnetospheric magnetic field: Methods and results, *Space Sci. Rev.*, *54*, 75, 1990.

Tsyganenko, N. A., S. B. P. Karlsson, S. Kokubun, T. Yamamoto, A. J. Lazarus, K. W. Ogilvie, C. T. Russell, and J. A. Slavin, Global configuration of the magnetotail current sheets as derived from Geotail, Wind, IMP 8 and ISEE 1/2 data, *J. Geophys. Res.*, *103*, 6827, 1998.

Vaisberg, O. L., et al., Complex plasma spectrometer SKA-1, in *INTERBALL Mission and Payload*, edited by dont know, vol. 12345, p. 170, 1995.

Vaisberg, O. L., et al., Initial observations of fine plasma structures at the flank magnetopause with the complex plasma analyzer SCA-1 onboard the Interball tail probe, *Ann. Geophysicae*, *15*, 570, 1997.

Van Leer, B., Towards the ultimate conservative difference scheme. III. Upstream centered finite difference schemes for ideal compressible flow, *J. Comp. Phys.*, *23*, 263, 1977.

Vasyliunas, V. M., Electrodynamics of the ionosphere/magnetosphere/solar wind system at high latitudes, in *NATA Advanced Studies Inst.*, Lillehammer, 1988.

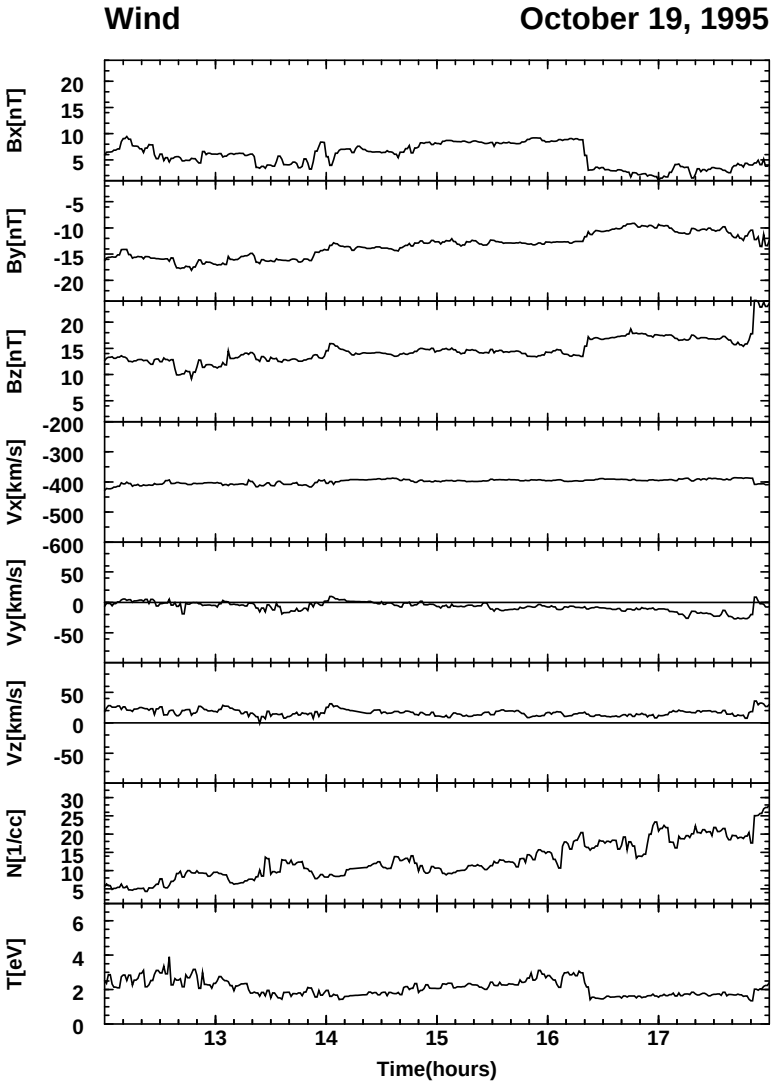

Figure 1: Wind solar wind and IMF observations, showing from top to bottom: the three magnetic field components B_x, B_y, and B_z, the three plasma velocity components V_x, V_y, and V_z, the plasma number density N, and the plasma temperature T. All quantities are in GSM coordinates.

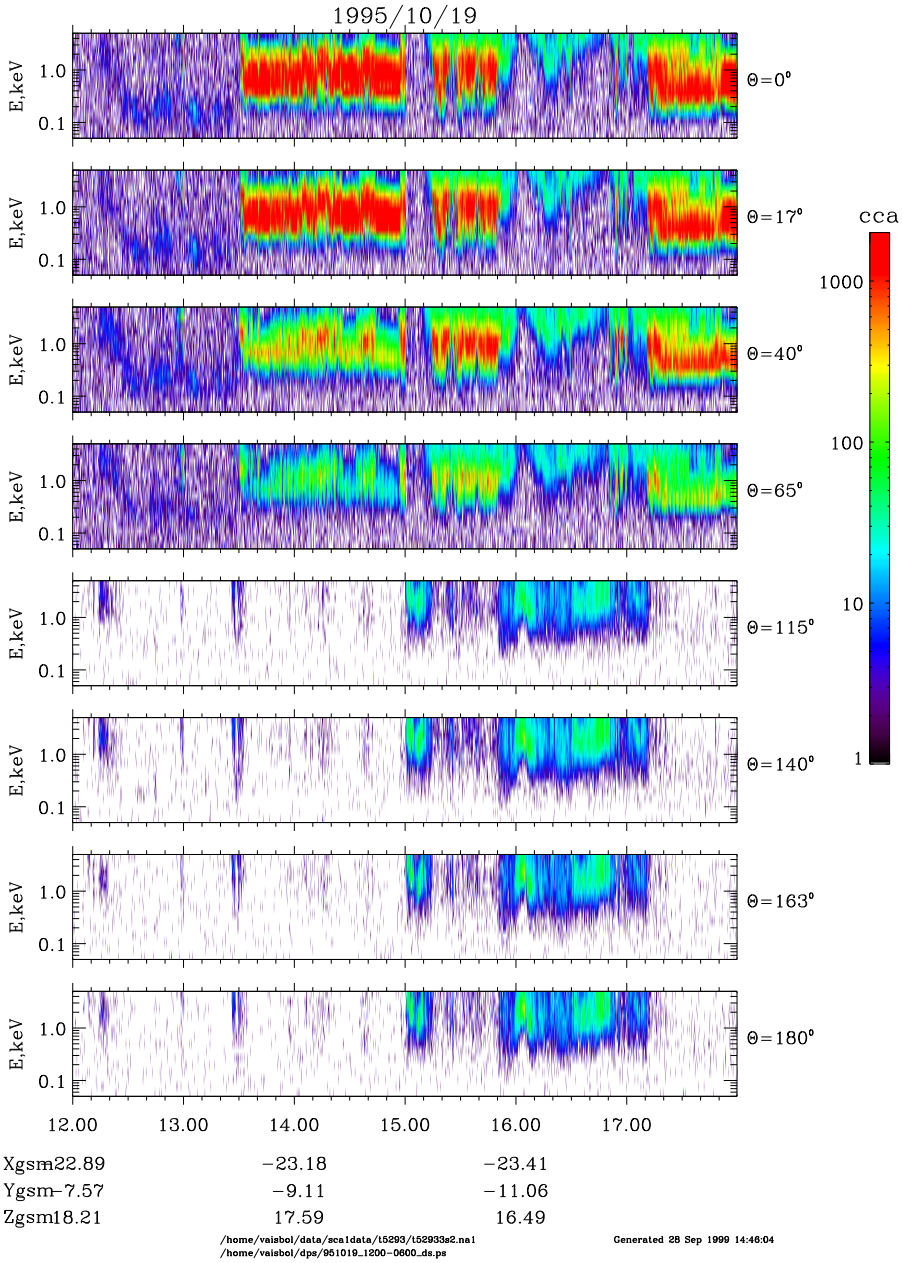

Figure 2: Energy-time spectograms from the Interball tail probe. See text for details.

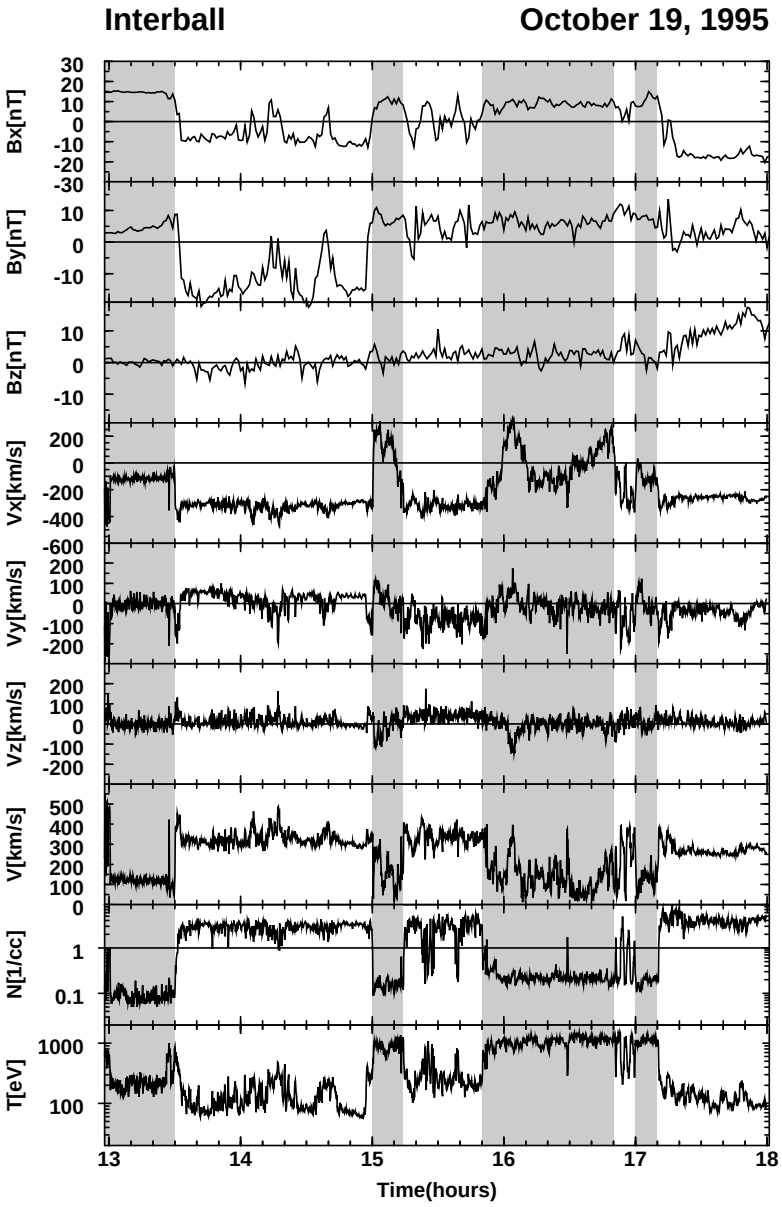

Figure 3: Interball plasma and field observations, showing from top to bottom: the three magnetic field components B_x, B_y, and B_z, the three plasma velocity components V_x, V_y, and V_z, the plasma number density N, and the plasma temperature T. All quantities are in GSE coordinates. The shaded intervals indicate times when Interball observes lobe-like plasma and fields.

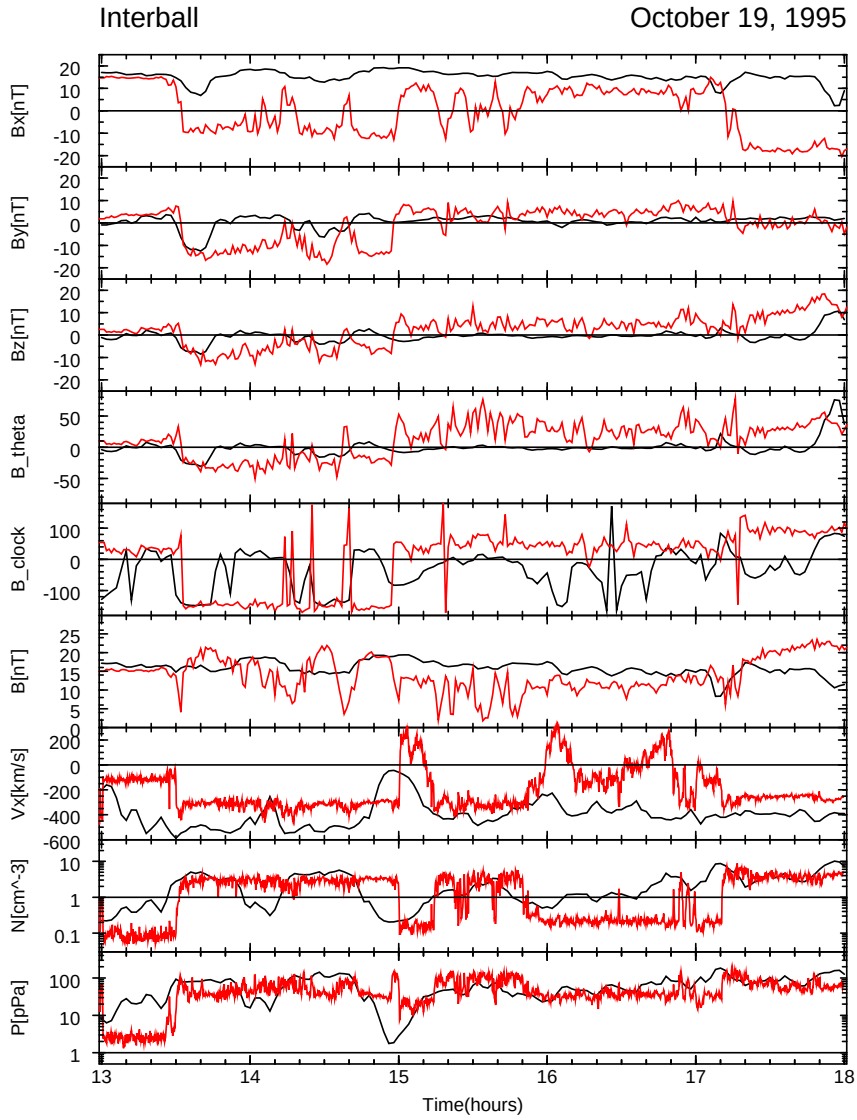

fig4

Figure 4: Comparison between the Interball observations (red lines) and time series taken from the simulation (black lines), the three magnetic field components B_x, B_y, and B_z, the magnetic field elevation angle B_theta, the magnetic field clock angle B_clock, the X component of the plasma velocity V_x, the plasma number density N, and the plasma pressure P. All quantities are in GSE coordinates.

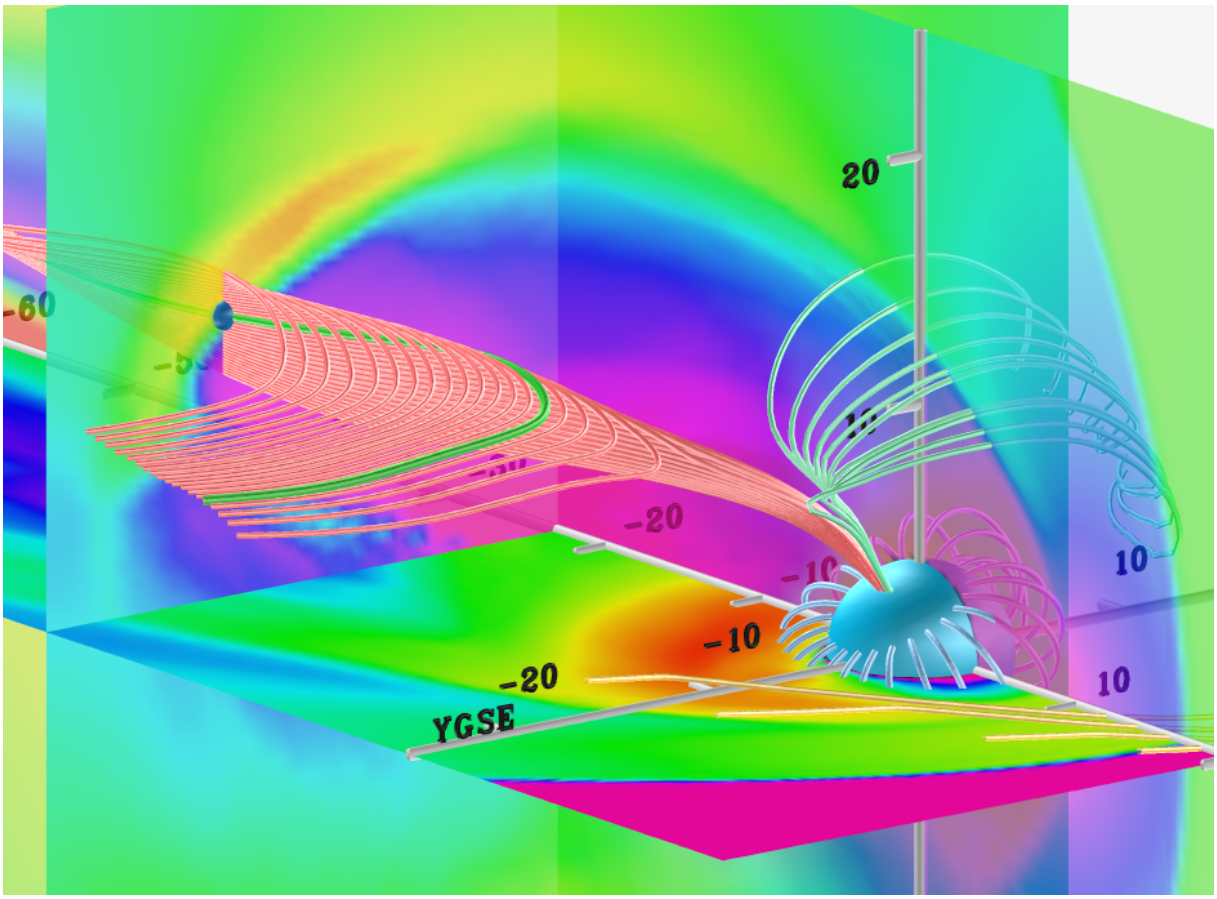

Figure 5: Three-dimensional rendering of the simulated magnetosphere. See text for details.

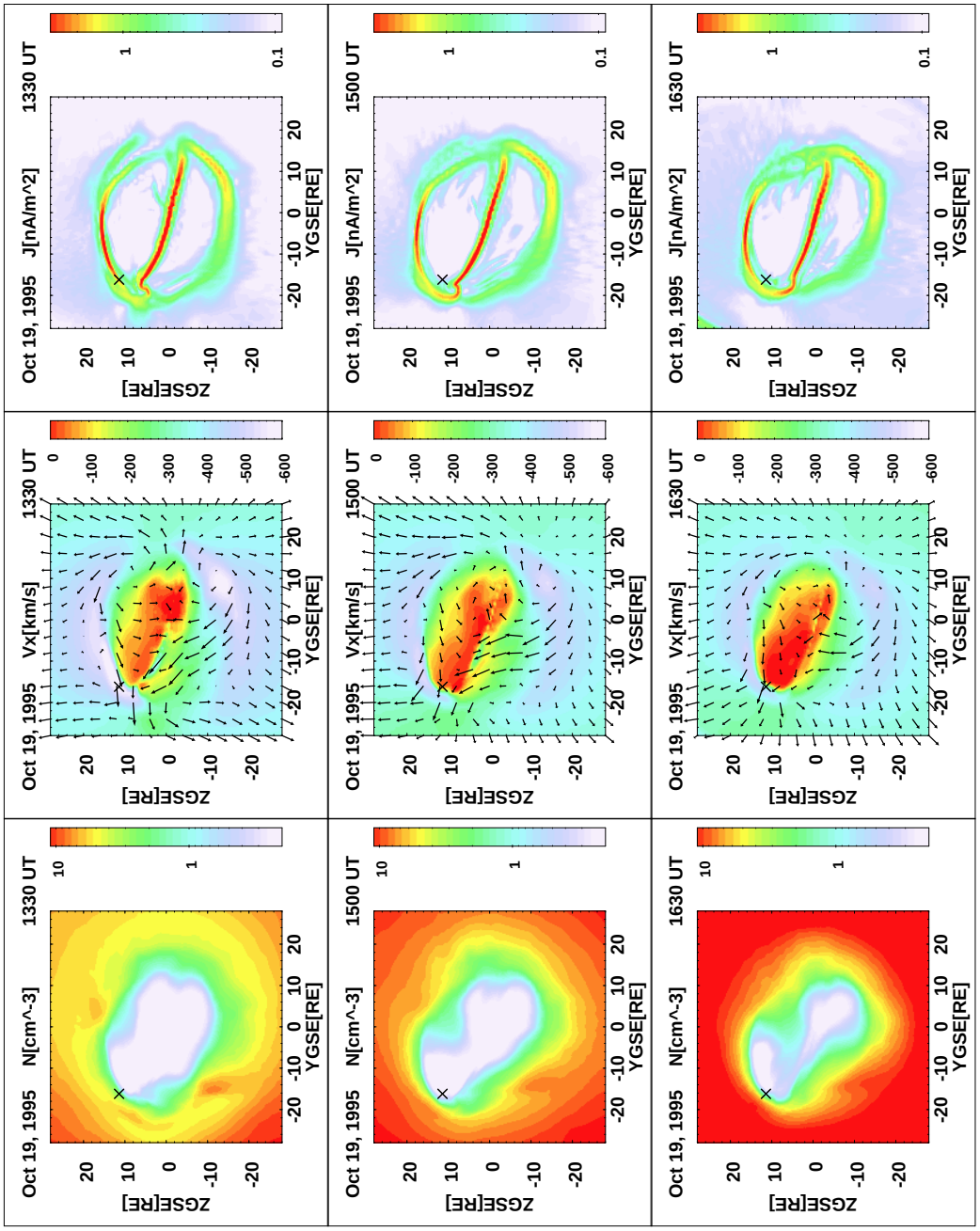

Figure 6: Cross sections of the tail plasma parameters number density, velocity, and current density, at 1330, 1500, and 1630 UT, respectively. The cross sections are taken in the Y-Z plane at X=-23.1 R_E, i.e., the plane through Interball. The black cross marks the Interball position. The longest velocity arrows represent 150 km/s.

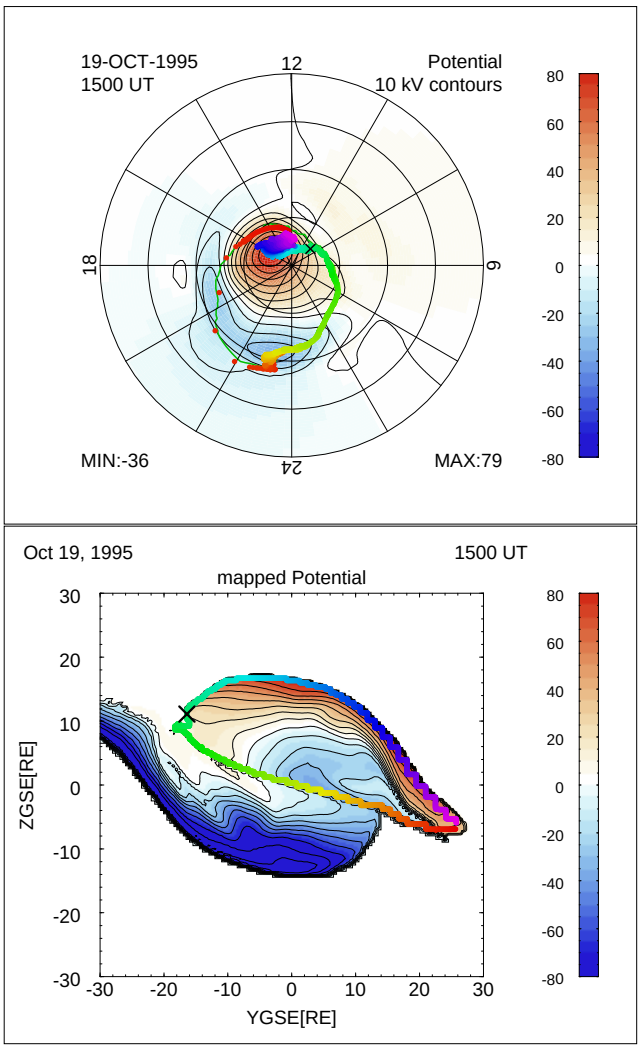

Figure 7: Upper panel: Ionospheric potential at 1500 UT. The black cross marks the magnetic footpoint of Interball. The green line is the polar cap boundary, i.e., the boundary between open and closed field lines. Lower panel: The ionospheric potential mapped to the Y_{GSE} - Z_{GSE} plane at the Interball position (X_{GSE}=-23.1 R_E). The black cross marks the Interball position. The colored dots indicate the magnetic mapping of field lines just inside the magnetopause between the plane and the ionosphere.